Surface & Coatings Technology 507 (2025) 132095

Contents lists available at ScienceDirect

Surface & Coatings Technology

journal homepage: www.elsevier.com/locate/sct

Full length article

Convergence during feedback controlled reactive magnetron sputtering: Mechanisms and classification

J. Van Bever [a], K. Strijckmans [a], S. Konstantinidis [b], D. Depla [a,*]

[a] Department of Solid State Sciences, Ghent University, Krijgslaan 281 (S1), 9000 Gent, Belgium
[b] Plasma-Surface Interaction Chemistry (ChIPS), University of Mons, Place du Parc 20, 7000 Mons, Belgium

ARTICLE INFO

Keywords:
Reactive sputtering
Feedback control
Voltage stabilization

ABSTRACT

During feedback control of reactive magnetron sputtering, process parameters often exhibit a complex time-dependent behavior. This behavior hinders process stabilization and can lead to a modification of the desired film properties. This study investigates the processes behind this behavior by performing time-resolved measurements during reactive sputtering of aluminum in argon/oxygen mixtures. Two distinct groups of physical processes were identified. The first group exhibits a relatively fast time-dependent behavior, leading to process stabilization within 5 to 8 min. This group includes processes related to reactive gas introduction, its interaction with deposited material, and the feedback loop characteristics. The second group causes a continuous drift of the process for more than 45 min, primarily due to oxide deposition on the chamber walls and target erosion. These two groups have a different impact on the process curves known as hysteresis curves. For the first group, the impact is minimal while for the second group the hysteresis curve becomes distorted, potentially leading to misinterpretation or incorrect selection of deposition conditions. The utilization of the difference between the discharge voltage and floating potential as the feedback input signal eliminates the impact of oxide deposition and mitigates this problem.

1. Introduction

High-quality compound coatings can be produced by reactive magnetron sputtering, a deposition technique based on a magnetically confined gas discharge between a cathode and an anode. The cathode or target is the source of the metal constituent to be deposited. The anode includes often the substrate and/or chamber walls. A reactive gas, such as oxygen or nitrogen, is added to the process and forms with the deposited metal the desired compound coating. Depending on the experimental conditions, a compound layer can also form on the target, which significantly influences the deposition process.

Fig. 1 shows a schematic of a process curve, as can be observed during the reactive sputtering of aluminum with oxygen as reactive gas. This reactive gas/metal combination is used in this work. The process curve defines three different modes which are related to the target surface condition. When the target surface is mainly metallic, the process is in the "metallic mode" (blue). A fully oxidized target is related to the "poisoned mode" (red). The "transition mode" (purple), in which the target surface is partially oxidized, connects the other two modes. The transition mode is the most interesting mode for the high-rate deposition of high-quality compound coatings [1,2], but also the most challenging mode to control the process.

The reactive sputtering process can be controlled in two ways. During direct flow control, the oxygen flow is defined by a fixed setting of the flow controller. When applying direct flow control within the example shown in Fig. 1, the process will switch from metallic to poisoned mode (↓) when increasing the oxygen flow beyond the first critical point (▽). The reverse transition (↑) will occur when lowering the oxygen flow below the second critical point (×). As both transition points do not coincide, this type of process curve is known as a hysteresis curve. Due to the hysteresis behavior, the transition mode is often not stable in flow control. Specific process conditions, such as using a high-pumping speed [3,4], can be applied to avoid hysteresis, but are often less cost-effective and undesired for industrial applications [1,5]. An alternative process control method was therefore developed to access the transition mode, in which a feedback loop is used to indirectly control the reactive gas flow [1,6–13]. The input of the feedback loop is one or more deposition variables such as the deposition rate, the discharge voltage, the reactive gas partial pressure, and an emission line intensity. In this work, voltage-based feedback control was used, which is from a technical perspective the easiest solution to investigate the physics that influence the feedback convergence. These physics should also influence feedback control based on more

* Corresponding author.
E-mail address: diederik.depla@ugent.be (D. Depla).

https://doi.org/10.1016/j.surfcoat.2025.132095
Received 20 February 2025; Received in revised form 25 March 2025; Accepted 26 March 2025
Available online 9 April 2025
0257-8972/© 2025 Elsevier B.V. All rights are reserved, including those for text and data mining, AI training, and similar technologies.

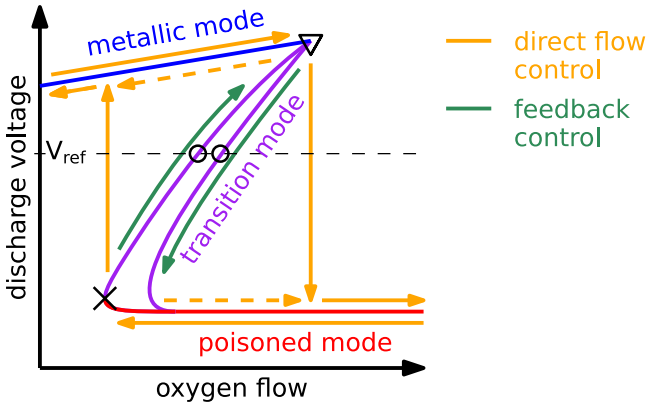

Fig. 1. Schematic of a hysteresis curve during the reactive sputtering of aluminum with oxygen. Indicated are: the different sputtering modes (metallic, transition and poisoned), the first critical point (▽), the second critical point (×), the control modes (direct flow, feedback) and the reference voltage (V_{ref}) with its corresponding steady-state conditions (○). Dashed lines indicate direct flow control specific for the procedure followed in this paper. The concepts are explained in the text.

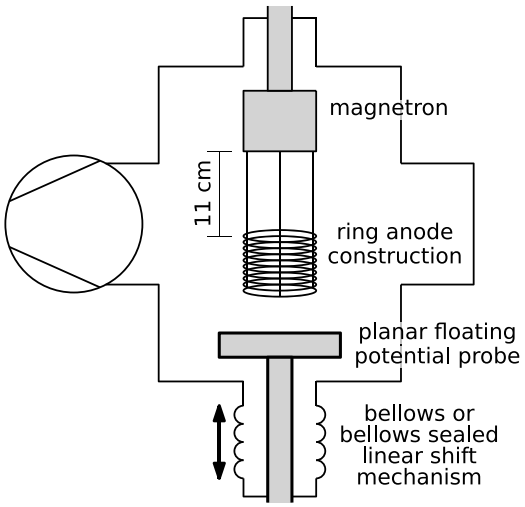

Fig. 2. Schematic of the chamber including the anode constructions and the floating potential probe developed in previous work [17].

complex feedback input signals. The value of an input signal is known as the setpoint or reference value (Fig. 1, V_{ref}). Based on modeling and experiments, our team has shown that the transition state can have two different values depending on whether the process was prepared in metallic or poisoned mode (Fig. 1, ○), which is termed "double hysteresis" [14–18]. We will therefore distinguish between feedback control starting from either the metallic or poisoned mode. While feedback control provides an essential tool to access the transition mode, maintaining a stable process condition during feedback control remains still challenging.

The problem of maintaining a stable process condition originates from processes that change the process conditions during the feedback control. Examples are the evolution inherent to the feedback loop algorithm itself [8,9], changes in reactive gas pressure [19], arcing [20–22], target erosion [23,24] and the physics related to the deposition of an insulating coating onto the anode [1,17,25]. When the input signal of the feedback loop continuously changes due to such processes, slow drifting of other process parameters will be induced by the feedback loop as the loop enforces a constant input signal. Such drifting was reported when using the discharge voltage [1,17] or an optical emission line intensity [26] as input. While much is known from literature on each of the individual processes, no consistent study was found on their interplay. This is a problem when trying to achieve and maintain a stable process condition in transition mode, because all aforementioned processes happen simultaneously, each influencing the convergence towards a stable process condition in its particular way.

In this work, the processes that change the oxygen flow, discharge voltage and gas pressure during reactive magnetron sputtering are approached in a systematic way. We present time-resolved measurements of the oxygen flow, gas pressure, discharge voltage, and floating potential during the feedback-controlled reactive sputtering of aluminum in argon/oxygen mixtures, and use these measurements to classify the processes. We then shift from a paradigm, in which the processes are described due their effect in time, to a paradigm, in which the processes are related to the hysteresis curve. This provides a powerful tool to understand their interplay and to minimize the efforts that are needed to achieve and maintain a stable deposition condition in transition mode.

2. Experimental

The set-up consists of a stainless steel chamber that has a cross shaped design, with axes of length 34, 35 and 48 cm and diameter 20, 15 and 15 cm respectively. Circular aluminum targets (99.999%), 50.8 mm in diameter and 3 mm in thickness (Testbourne Ltd.) were mounted on a home-built magnetron source that was powered in direct current (DC) mode by a TruPlasma DC 4001 power supply (Trumpf Hüttinger). A turbomolecular pump (TMH521P, Pfeiffer Vacuum) was connected to the chamber using a gate valve to control the pumping speed. Argon and oxygen were introduced using a 50 sccm (standard cubic centimeters per minute) MKS and a 10 sccm MicroFlo mass flow controller respectively. The MicroFlow controller, which was used for the feedback control, had a response time of 40 ms. The oxygen flow was controlled with a Speedflo system (Gencoa). The total gas pressure was measured using a capacitance gauge (CMR 375), controlled by a TPG362 unit (Pfeiffer Vacuum).

Improved stability of the feedback control was observed when using anode constructions that have a large effective area (Fig. 2). Therefore, at the bottom of the chamber, bellows or a bellows sealed linear shift mechanism were mounted. For some measurements, also a construction of 10 copper rings (inner diameter 63 mm, outer diameter 82 mm, thickness 2 mm and separation 1.2 mm) was mounted at a distance of 11 cm to the target using 3 stainless steel rods of diameter 3 mm. The latter construction also confines the plasma in front of the target [27,28]. The setup with the ring anode construction is indicated in the paper with "setup A".

For some measurements, a planar floating potential probe was used to monitor the floating potential shift due to oxide deposition [17]. The probe was fixed at a distance of either 22.5 or 24 cm from the magnetron (Fig. 2). The floating potential was measured using a DMM6500 6½ Digit Multimeter (Keithley). For technical reasons, the aforementioned ring anode construction was removed when the probe was used, while the bellows were kept in place. The setup with the probe is indicated in the paper with "setup B".

Feedback control was applied using either the discharge voltage or the difference of discharge voltage and floating potential as the feedback input signal. The Speedflo system implements an adapted version of the Pseudo-Derivative-Feedback (PDF+) control loop algorithm [29–32] for feedback control. Three parameters define the integrated part ($K1$), the derivative part ($K2$) and the higher order pseudo-derivative part of the algorithm. The values of $K1$ and $K2$ were manually optimized for the fastest convergence and best stability. A value of $K1 = 0.7$ was used in all measurements shown. A larger chamber or higher discharge current typically requires a larger value of $K1$ for stabilization but it was observed that a higher $K1$ also results in larger temporary fluctuations of the process parameters. The

corresponding value of $K2$ was chosen as large as possible to obtain fast feedback, but is also limited by stability requirements. The value of $K2$ was set to $K2 = 3 \times 10^{-4}$, unless there was a large difference between initial and setpoint voltage (as for some measurements in Section 3.2.1) or when the difference of discharge voltage and floating potential was used ("setup B"), in which case it was set to $K2 = 7 \times 10^{-5}$. The parameter corresponding to the higher order pseudo-derivative part of the PDF+ algorithm was set to its default value (0.05).

A LabView interface was used for the digital communication with the power supply, the DMM6500 multimeter and the TPG 362 control unit (resulting in a precision of approximately 4×10^{-4} Pa). Data was also retrieved from the SpeedFlo reactive feedback control system. A Python code was developed to synchronize all actions and for post-processing. When using the difference of discharge voltage and floating potential as feedback input signal, the analog output from the power supply was combined with the digital output from the DMM6500 and sent to the analog input of the Speedflo system using a NI USB-6008 device. This resulted in an additional loop time. The feedback control was observed to become unstable if this additional loop time exceeds 100 to 300 ms, which is in agreement with limits found in literature [6,8,9]. After optimization of the floating potential signal processing, the additional loop time was reduced to 60 ms, resulting in stable feedback on the difference of discharge voltage and floating potential.

As discussed before, the metal-to-poison transition follows a different path than the poison-to-metal transition. The experiments discussed in this paper will focus on the metal-to-poison transition. To achieve this (Fig. 1), the process is first conditioned in metallic mode using direct flow control (→). Next, the transition region is accessed using feedback control (↙). Finally, direct flow control is used in poisoned mode (⇢). The same observations as presented here were made for the reverse transition in which the process is initialized in poisoned mode, following the reverse path (←, ↗, ⇠). In this study, we also present hysteresis measurements, which are a combination of both measuring schemes. The curves were sampled step-wise, starting in metallic mode. The exact procedure is presented in the Supplementary information and is based on the knowledge acquired during this study.

A standardized conditioning procedure was applied to prepare the process in metallic mode, unless stated otherwise. First, sputter cleaning in pure argon is done (≥ 8 min). When the floating potential probe was mounted, a floating potential between 19 and 21 V was always observed after sputter cleaning. Then, sputtering at an oxygen flow 0.1 sccm below the first critical point is performed (≥ 4 min). When conducting hysteresis measurements, this conditioning was replaced by a step-wise sampling of the metallic mode using direct flow control.

The time derivatives reported in this work were calculated by straight line fitting through the data, using a sufficiently large time window to mitigate effects from temporary fluctuations. Occasionally, Lowess smoothing [33] of the data was used to assist in the derivative calculation.

All measurements shown were performed at the same argon flow (7 sccm) and argon pressure (0.4 Pa, measured without gas discharge). For the sake of completeness, this information is repeated in the figure captions. The corresponding pumping speed is between 32 l/s and 40 l/s. The base pressure at this low pumping speed was well below 3×10^{-3} Pa (measured with a PKR 251 compact full range gauge, Pfeiffer Vacuum) for all measurements.

3. Results

Processes during the convergence of feedback control are investigated using the reactive sputtering of aluminum in an argon/oxygen mixture as prototype system. We first show how feedback control, using the discharge voltage as input signal, results in a protracted and intricate convergence of the process parameters (Section 3.1). Next, individual processes are examined (Section 3.2). This knowledge is then applied in a detailed time-analysis of feedback control convergence (Section 3.3). Finally, the processes are classified based on their impact on the feedback convergence (Section 4).

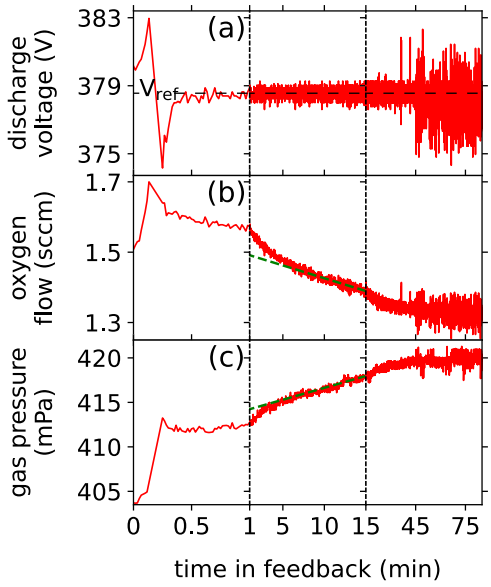

Fig. 3. Process variables as a function of the time in feedback control: (a) the discharge voltage, (b) the oxygen flow, (c) the total gas pressure. The time axis is subdivided to distinguish processes discussed in this work. The value of the reference voltage is indicated with a dashed line in the top panel. Green dashed lines are used to guide the eye. Process parameters: discharge current = 0.35 A, DC, argon flow = 7.0 sccm, argon pressure = 0.40 Pa. Setup: A.

3.1. Feedback convergence using the discharge voltage as the feedback input signal

The convergence of different process parameters during feedback control can be both slow and complicated. To illustrate this, the time evolution of discharge voltage, oxygen flow and total gas pressure is monitored during feedback control (Fig. 3). The feedback loop used a constant discharge voltage of approximately 379 V as the reference voltage ("V_{ref}"), at which the process is brought in transition mode. Since changes occur on different time scales, the time axis of Fig. 3 is divided into three segments. It is observed that convergence towards a constant value significantly varies among the three process parameters. The reference voltage is achieved within the first minute (Fig. 3a). The oxygen flow and gas pressure, however, converge more slowly, reaching only a constant value after approximately 35 min (Fig. 3b–c). Instabilities due to arcing emerge after 45 min, limiting the stable process conditions to a brief window of 10 min. To better understand these changes, the following section describes tailored experiments designed to illuminate specific aspects of the time evolution.

3.2. Processes influencing the feedback convergence

3.2.1. Reference voltage approaching by the loop control

While the reference voltage is quickly reached (Fig. 3a), it is worth investigating whether the method to approach of the reference voltage also impacts the convergence of the other process parameters. Fig. 4 shows the time evolution of three experiments in which feedback control is used to approach a reference voltage of 330 V.

In a first experiment, after sputter cleaning in pure argon, the feedback control is immediately initiated ("none", red curves). It is observed that the oxygen flow increases steadily beyond the value at the first critical point (Fig. 4b, 0–1 min) which, under the given conditions, corresponds to 2.1 sccm. To force the process into transition mode, this flow must be exceeded, causing the discharge voltage to drop and triggering the feedback control to adjust the oxygen flow. This behavior aligns with theoretical predictions, including the damped oscillation of the feedback input signal (Fig. 4a, 0–3 min) [8]. The

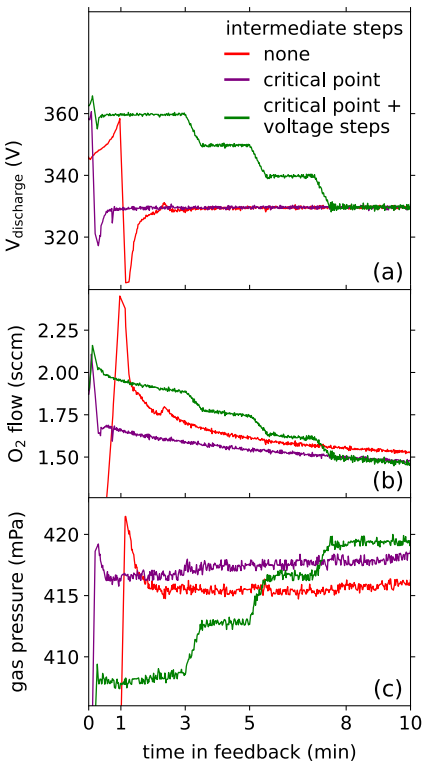

Fig. 4. Impact of adding intermediate steps (see legend) between process conditioning and feedback control with a reference voltage of 330 V: (a) discharge voltage, (b) oxygen flow, (c) total gas pressure. Process parameters: discharge current = 0.5 A, DC, argon flow = 7.0 sccm, argon pressure = 0.40 Pa. Setup: A.

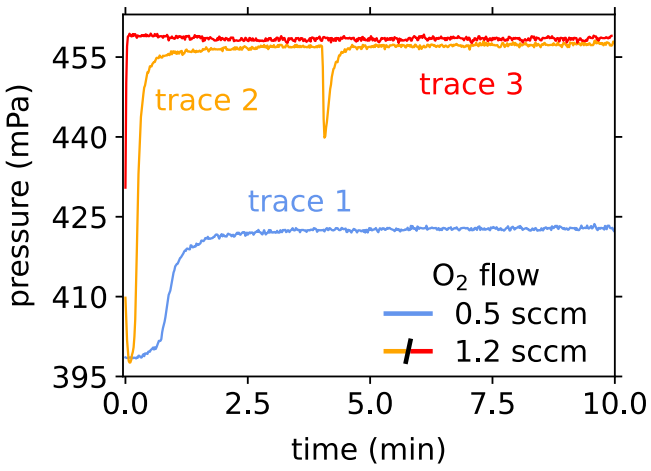

Fig. 5. Effect on the gas pressure evolution due to the introduction of oxygen without a gas discharge. Process parameters: argon flow = 7.0 sccm, argon pressure (without discharge) = 0.40 Pa. Setup: A.

exact time required for oscillation suppression depends on the feedback parameters $K1$ and $K2$.

In a second experiment (purple curves), instead of directly approaching the reference voltage, the process was held for 4 min at approximately 0.1 sccm below the first critical point before the feedback control was started (purple curves). This adjustment significantly reduces the oxygen flow overshoot (Fig. 4b, 0-30 seconds) and the discharge voltage oscillation (Fig. 4a, 0-45 seconds). Additionally, during the first few minutes of feedback control (1–5 min), a reduced time derivative of the oxygen flow evolution was observed (Fig. 4b), alongside lower oxygen flow values and a higher gas pressure (Fig. 4b-c). The latter indicates that a more converged process condition is obtained as more time will be required in the first experiment to achieve the same oxygen flow and gas pressure.

In a third experiment (green curves), the process is not only fixed near the critical point before the feedback control is started, but also the reference voltage was adjusted stepwise towards its final value of 330 V. Between each step, the reference voltage was ramped over 30 seconds. The discharge voltage closely followed the intermediate reference voltage (Fig. 4a). The following observations can be made. First, the stabilization of the discharge voltage value takes only 30 seconds, with minimal overshoot in discharge voltage, oxygen flow and gas pressure (Fig. 4). Second, feedback stability improves, enabling the feedback parameters $K1$ and $K2$ to be adjusted to speed up loop control. Third, multiple process conditions can be sampled sequentially without re-initializing feedback convergence. This is evident in Fig. 4b, where the time derivative is approximately equal during the reference voltage steps (green curve, excluding the steep ramps around 3, 5 and 7 min) compared to a single reference voltage (purple curve). Finally, gas pressure convergence improves, with a smaller slope and higher value of the gas pressure after 8 min (Fig. 4c). The latter is beneficial as the system tries to converge towards higher pressures (as seen in Fig. 3c), which can be understood from the pressure-flow correlation within the transition region [1].

In summary, while the reference voltage is achieved by the loop control within approximately 1 minute, the method to approach to this reference voltage significantly impacts the evolution of oxygen flow and gas pressure.

3.2.2. Gas distribution and gas–wall interactions

A change in the gas flow will induce pressure variations, and even in the absence of a discharge, the pressure needs to stabilize. In this section, it is investigated how the chamber wall condition and the applied oxygen flow rate influence the pressure stabilization. In a first experiment, before oxygen addition, the target was sputtered in pure argon for 12 min, after which the discharge was turned off and 0.5 sccm of oxygen is added into the chamber. Fig. 5 shows that the pressure quickly stabilizes (trace 1, blue line). This experiment is now repeated by introducing 1.2 sccm of oxygen after 7 min of sputtering in pure argon (trace 2, orange line). The pressure increases much faster as compared to the first experiment. A dip is sometimes observed around 4 min. While the exact cause of this transient behavior remains unclear, its effect on the remainder of the measurement is negligible. In a third experiment (trace 3, red line), only the oxygen flow was interrupted for 5 min, after which the oxygen flow was set to its original value of 1.2 sccm. The pressure almost instantaneously stabilizes.

The slowest pressure evolution is observed at lower oxygen flow rates and after thorough sputter cleaning in pure argon (trace 1), though even in this case, a stable pressure is quickly reached. After 5 to 8 min, no measurable pressure changes exceeding the precision of 5×10^{-4} Pa are observed. Additionally, the final pressure is already approached within 1×10^{-3} Pa (or 0.05% of the final oxygen pressure) during the first 3 min. Conversely, achieving the same precision in the feedback measurement, as shown in Fig. 3c, requires over 25 min. The fastest pressure stabilization is observed when only the oxygen flow is turned off between experiments (trace 3). The negligible delay in pressure increase indicates that not only the distribution of the gas within the chamber, but also the interaction of the gas with the chamber walls govern the process evolution within the first 5 to 8 min after a gas flow change.

In summary, changes of oxygen flow result in a brief relaxation of the process that occurs independently of the use of feedback control. These relaxation processes are likely governed by a combination of the distribution of the gas into the chamber and the interaction of the oxygen with the layer deposited on the chamber walls. Stabilization is consistently observed within 1 to 8 min after the process change.

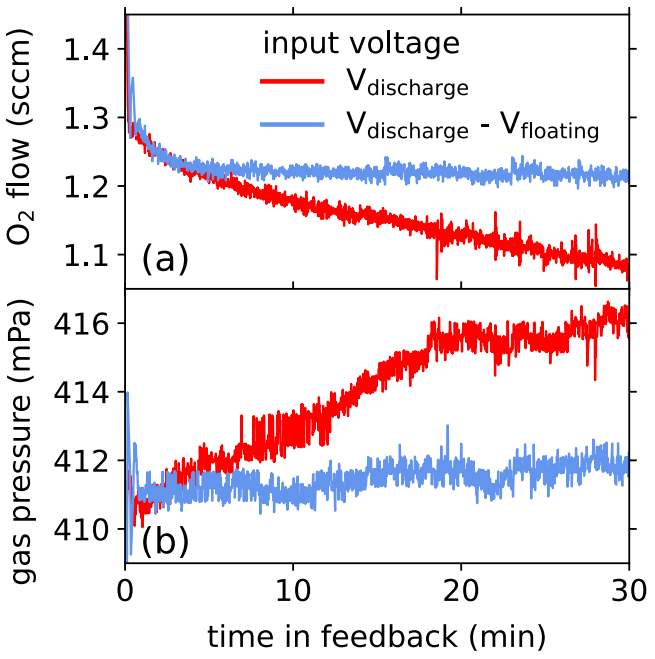

Fig. 6. Effect of the feedback input signal (legend: $V_{discharge}$ = discharge voltage, $V_{floating}$ = floating potential) on (a) the oxygen flow and (b) the total gas pressure. Process parameters: discharge current = 0.35 A, DC, argon flow = 7.0 sccm, argon pressure = 0.40 Pa. Setup: B.

3.2.3. Oxide deposition

As shown in Fig. 3, the oxygen flow and gas pressure only stabilize after an extended period (>30 min). This drift can be explained by our previous work [17], which demonstrated that the deposition of an oxide coating on the chamber walls leads to an increase in discharge voltage. As the feedback loop aims to keep the reference voltage constant, the drift of the discharge voltage is compensated by changing the oxygen flow, and as a consequence the oxygen pressure.

Our previous work [17] also showed that the floating potential drifts in the same way as the discharge voltage, and hence the difference between the discharge voltage and the floating potential remains constant. It is therefore expected that, when the latter difference is used as the input signal for the feedback control loop, the oxygen flow and the total gas pressure will converge much faster. To illustrate this, Fig. 6 compares the time evolution of the process parameters when, after standard conditioning of the process (Section 2), feedback control is started using either the discharge voltage (red curve) or the difference between discharge voltage and floating potential (blue curve) as the feedback input signal. The reference voltage of the feedback control was set to 340 V when using the discharge voltage as input and 320 V when using the voltage difference as input. The 20 V offset compensates for the floating potential after chamber conditioning (19–21 V), ensuring that both feedback procedures start at a comparable oxygen flow.

As expected from the already presented experiments (Section 3.1), the oxygen flow drifts over 30 min when the discharge voltage is used as the feedback input signal (Fig. 6a, red curve). Quantitatively, the oxygen flow decreases by -7×10^{-5} to -9×10^{-5} sccm/s. Conversely, using the voltage difference as input signal results in a significantly faster convergence (Fig. 6a, blue curve). Within just 5 min of feedback using the voltage difference as input, the time derivative of the oxygen flow stabilizes between -4×10^{-6} and -8×10^{-6} sccm/s. The changes observed during the first 3 to 5 min under voltage difference-based feedback control are attributed to gas introduction and gas–wall interaction, as previously discussed (Section 3.2.2). These results indicate that the original drift in the oxygen flow and total pressure is caused by the impact of oxide deposition on the discharge voltage.

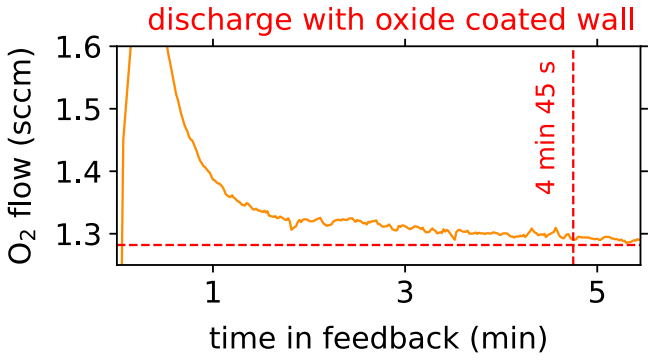

Fig. 7. Convergence of the oxygen flow when the chamber wall is pre-coated with oxide for 3 h. Process parameters: discharge current = 0.35 A, DC, argon flow = 7.0 sccm, argon pressure = 0.40 Pa.

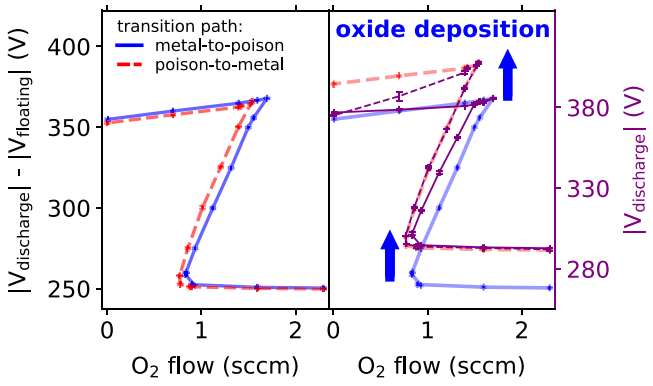

Fig. 8. Comparison of the hysteresis curve in difference of discharge voltage and floating potential (left pane) and the corresponding curve in discharge voltage (right pane). The transition paths of the left pane are deliberately shifted and redrawn in the right pane. The obtained discharge voltage is the result of a vertical movement of the blue and red curves to higher voltages (blue arrows). Process parameters: discharge current = 0.35 A, DC, argon flow = 7.0 sccm, argon pressure = 0.40 Pa. Setup: B.

An alternative way to demonstrate the effect of oxide deposition on the chamber walls is to first cover the chamber walls with an oxide layer prior to the start of the feedback control using the discharge voltage as the feedback input signal. Therefore, the chamber was pre-coated with oxide by sputtering in transition mode for 3 h. Then, the discharge was turned off, and reignited five days later. To exclude the impact of target properties, the feedback control was preceded by sputter cleaning in pure argon. This intermediate step can be expected to have only a minor influence on the chamber state as its duration was limited to only 3 min. Feedback control with a constant reference voltage was applied, achieving an oxygen flow precision of 0.01 sccm within 4 min 45 s (Fig. 7, red dashed lines). Conversely, achieving the same precision starting from a metal-coated chamber wall requires 30 min (Fig. 3b, blue dashed lines). This further confirms that the long drift associated with oxide deposition is eliminated in Fig. 7. The remaining convergence time of 4 min 45 s can be attributed to the gas introduction and gas–wall interaction, as previously discussed.

In summary, oxide deposition causes a 30 minute drift of the oxygen flow and gas pressure during feedback convergence (Fig. 3). This drift can be eliminated, either by using a corrected discharge voltage signal as the feedback input (Fig. 6) or by preconditioning the chamber walls into an oxide coated state (Fig. 7).

One of the goals of this paper is to classify the observed processes based on their impact on a hysteresis experiment. Therefore, the impact of oxide deposition on the hysteresis curve is studied. As was shown in Fig. 6, a stable process condition can be achieved by using the difference of discharge voltage and floating potential as the feedback

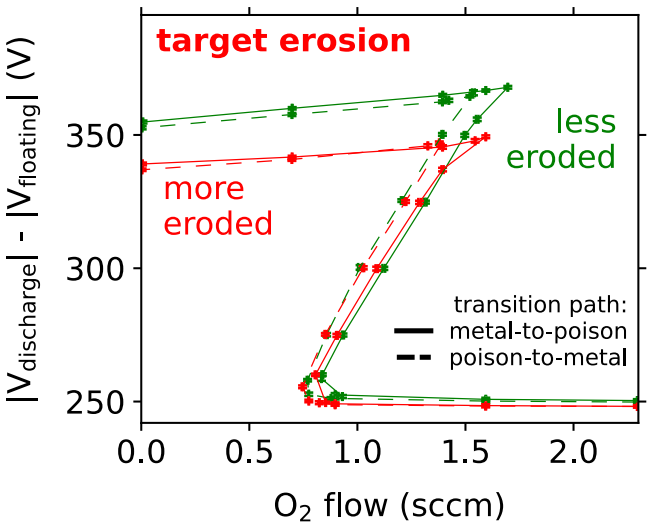

Fig. 9. Comparison of a hysteresis curve measured for a less eroded target (same data as in Fig. 8, left pane) with one obtained using a more eroded target (red curve). Process parameters: discharge current = 0.35 A, DC, argon flow = 7.0 sccm, argon pressure = 0.40 Pa. Sputtering time between the two measurements: 220 min, out which 79 min in metallic mode. Setup: B.

input signal. This input signal is therefore used to measure a hysteresis curve (Fig. 8, left pane). The right pane of Fig. 8 (purple curve) shows the discharge voltage data obtained during this measurement. To facilitate the comparison between both curves, the metal-to-poison transition path (blue curve) is repeated on the right pane and aligned with the metallic mode. This comparison shows that by the time the process reaches poisoned mode, the discharge voltage is shifted to a higher value. When the poison-to-metal transition path (red curve) is aligned with the poisoned mode in the right pane, one can observe the same voltage increase when entering back the metallic mode. The discharge voltage decreases again due to metal deposition when one further decreases the oxygen flow.

3.2.4. Target erosion

Even when using the difference between the discharge voltage and the floating potential as the feedback input signal (Fig. 6), a small decrease in oxygen flow, ranging between -4×10^{-6} and -8×10^{-6} sccm/s, remained. The remaining decrease can be attributed to target erosion. To proof this statement, the impact of target erosion on the hysteresis curve is studied. Fig. 9 compares a hysteresis curve for a less eroded target (green curve) with a hysteresis curve obtained for a more eroded target (red curve). Target erosion causes the hysteresis curve to contract from a "big Z" to a "small z", as shown by other researchers [23,24], inducing a slight but noticeable shift towards lower oxygen flows when initiating feedback from metallic mode (solid curves). Division of this oxygen flow shift by the sputtering time in between the two hysteresis measurements, yields an oxygen flow derivative between -2×10^{-6} and -7×10^{-6} sccm/s. This value matches the derivative calculated from Fig. 6a.

As a side note, it can be remarked that the poison-to-metal transition of the hysteresis curve (Fig. 9, dashed curves), shown for the more eroded target, shifts towards higher oxygen flows. Hence, if one would initiate feedback control from poisoned mode, target erosion would lead to an increase of the oxygen flow during feedback control.

In summary, target erosion causes a small drift of the oxygen flow (order 10^{-6} sccm/s), which remains when the impact of other processes is eliminated. The oxygen flow can either in- or decrease depending on the previous target state and chosen reference voltage.

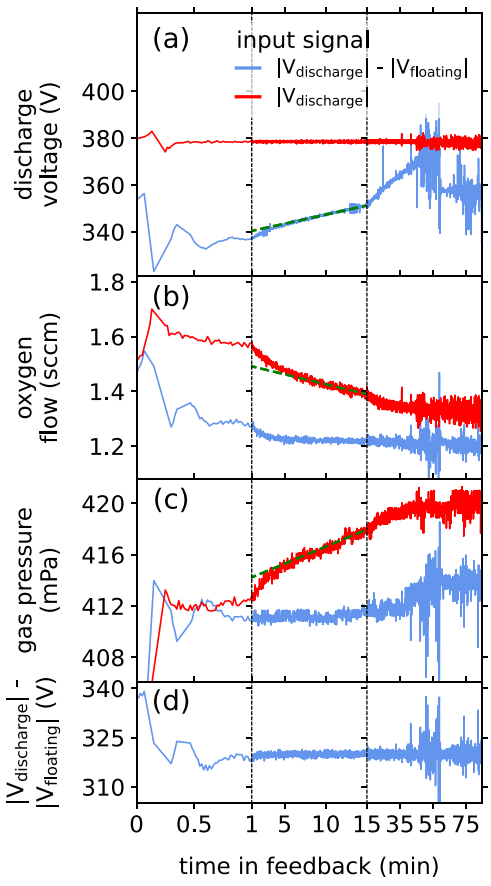

Fig. 10. Process variables as a function of time in feedback when using either the discharge voltage (red curve) or the difference of discharge voltage and floating potential (blue) as feedback input signal: (a) oxygen flow, (b) discharge voltage, (c) total gas pressure, (d) difference of discharge voltage and floating potential. The time axis is subdivided to identify the time windows discussed in the text. Process parameters: discharge current = 0.35 A, DC, argon flow = 7.0 sccm, argon pressure = 0.40 Pa. Setup: A (red curve) or B (blue curve).

3.3. Time-analysis of feedback convergence

With the knowledge obtained in the previous sections, it is now possible to review the different processes and define for each process a time window. This review will be made based on the time evolution during feedback covergence lasting for 85 min using the two discussed feedback input signals, i.e. the discharge voltage and the difference of the latter and the floating potential. Following time windows can be defined:

(i) 0–1 min: the feedback input signal, whether it is the discharge voltage (Fig. 10a) or the voltage difference (Fig. 10d), is rapidly stabilized by the feedback loop control.

(ii) 1–8 min: gas distribution and gas–wall interaction require a decrease of the oxygen flow to stabilize the discharge condition (Fig. 10b). When the discharge voltage is used as input signal, this decrease is superimposed with the effect of oxide deposition. During this period, a curvature is also observed in the evolution of either the gas pressure (Fig. 10c, red curve) or the discharge voltage (Fig. 10a, blue curve) depending on the feedback input signal.

(iii) 1–45 min: oxide deposition onto the chamber walls causes the discharge voltage to increase (Fig. 10a, blue curve). When the discharge voltage is kept constant by the loop control (Fig. 10a, red curve), the oxygen flow is decreased accordingly (Fig. 10b, red curve). A lower oxygen flow correlates with a higher oxygen

pressure in transition mode [1,14,34], causing an increase in the gas pressure (Fig. 10c).

(iv) beyond 45 min: arcing occurs, observed as instabilities in the discharge voltage (Fig. 10a). Since the discharge voltage signal is used as (a part of) the feedback input signal, these instabilities induce temporary fluctuations in the oxygen flow (Fig. 10b) and gas pressure (Fig. 10c). Notably, the anode ring construction (Fig. 2) was not mounted when using the voltage difference as the feedback input signal to avoid interference with the floating potential probe, which likely explains why increased arcing is seen in the blue curves of Fig. 10.

(v) 15–60 min: even when the difference of discharge voltage and floating potential is used as the feedback input signal, a gradual change of about 3 mPa is observed in the gas pressure (Fig. 10c). This change is absent when there is no sputter deposition and is likely caused by a continuous oxide covering of each surface of the chamber and the impact this has on oxygen gettering.

(vi) beyond 60 min: even when using the difference of discharge voltage and floating potential as feedback input signal, and after the discharge voltage drift caused by oxide deposition has stabilized (Fig. 10a, blue curve), a small average decrease between -5×10^{-6} and -9×10^{-6} sccm/s is found in the oxygen flow due to target erosion. This drift is not reflected in the discharge voltage due to the loop control and is below the measurement precision for the gas pressure.

The defined time windows will depend on the process conditions and experimental set-up but, generally speaking, it can be expected that relatively the same observations will be made. Factors that are expected to change the exact time windows are e.g. the discharge current, the chamber volume, the pumping speed and the required precision.

4. Discussion

4.1. Classification of processes during feedback convergence

The shown experiments demonstrate the impact of different processes on the convergence of feedback controlled reactive magnetron sputtering and allow for their classification. To guide the discussion, a schematic of a hysteresis curve is used Fig. 11. The black curve is repeated from Fig. 1 and is used as reference.

A first group of processes affecting the convergence, does not alter the reference hysteresis curve, but is related to the path the process follows to reach the reference voltage. Belonging to this group are the influence of the feedback loop control, the gas distribution and gas–wall interaction. When there is a significant difference between the initial process condition (Fig. 11, ×) and the condition corresponding to the reference voltage V_{ref} (black ○), the quick adaptation of the discharge voltage by the loop control leads to an unstable intermediate condition (△, green line). This intermediate state must then relax to a stable condition (black ○), which is influenced by the way the gas interacts with the deposited material on the chamber walls (orange line). The relaxation towards the stable condition is accompanied by a decrease in oxygen flow and, due to the shape of the hysteresis curve [1,14,34], an increase in gas pressure (Section 3.3). The relaxation process takes a short time ($\lesssim$ 8 min) and is expedited when intermediate steps are used (Section 3.2.1), keeping the process closer to a stable condition (Fig. 11, dashed gray line).

A second group of processes affecting the convergence, causes a modification of the reference hysteresis curve. As shown by our experiments, the change can be caused by oxide deposition (Section 3.2.3) and/or target erosion (Section 3.2.4). Oxide deposition results in an overall shift of the hysteresis curve, while target erosion leads to a deformation of the hysteresis curve (Fig. 11, blue and red arrows). As a consequence, the stable point (black ○) drifts (blue and red ○), accompanied by a gradual change in oxygen flow. The fundamental cause of these changes can be related back to changes of the discharge voltage–current relationships [17,23,24].

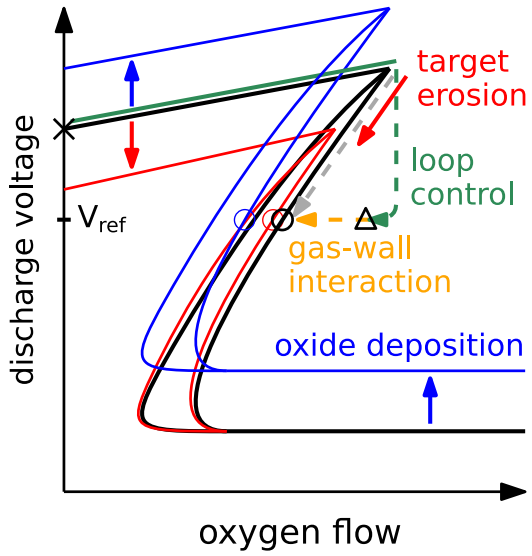

Fig. 11. Schematic of the hysteresis curve of the reactive sputtering of aluminum with oxygen, indicating the processes during feedback control. The feedback control is assumed to start in metallic mode (×), with the reference voltage (V_{ref}) corresponding to the state indicated by the black circle (○).

The exact drift depends on the process conditions and can be estimated from models [14,15,34–36]. For example, a change in pumping speed or argon pressure will alter the slope of the voltage–oxygen flow curve in transition mode. A shift of this curve towards higher voltages will therefore result in a slower or faster decrease of the oxygen flow, depending on the pumping speed and argon pressure.

The drifts caused by oxide deposition and target erosion complicate the attainment of a stable process condition, as longer deposition time exacerbate arcing-related instabilities (Section 3.3). However, these challenges can be mitigated by correcting the process parameters. For example, the impact of oxide deposition can be addressed by subtracting the floating potential (Fig. 6a). Similarly, literature describes a correction for target erosion, which changes the magnetic field at the target surface [23,24], achieved through the use of moving magnets [37].

4.2. Conditions achieved after feedback convergence

In this work, the results primarily focus on conditioning in metallic mode and bringing the process into the metal-to-poison transition using feedback control. Similar processes govern the feedback convergence when conditioning the target in poisoned mode (Fig. 1, red curve) and bringing the process into the poison-to-metal transition using feedback control. The conditions after feedback convergence differ, however, depending on whether the process starts in metallic or poisoned mode, even when the reference voltage is the same (Fig. 8, left pane, and Fig. 9). This phenomenon is known as double hysteresis [14–18]. The measured hysteresis curve complements the limited experimental evidence for double hysteresis. The purple curve in Fig. 8 aligns closely with the curves in Figure 2 of [18], providing strong confirmation and presenting a corrected shape for the transition mode (Fig. 8, left pane, and Fig. 9). Other observations of double hysteresis often stem from insufficient convergence of the processes discussed in this work. For instance, discrepancies may occur if the reference value is ramped too quickly [38,39]. To achieve reproducible measurement or deposition within the meta-stable transition mode, all processes outlined in this study must be properly accounted for when applying feedback control.

5. Conclusion

During reactive magnetron sputtering, time-dependent processes induce changes in reactive gas flow, gas pressure, and discharge voltage, which often hinder complete convergence of feedback control on the discharge voltage. These processes are classified into two distinct groups.

A first group comprises effects that induce the reactive sputtering process to gradually evolve towards the meta-stable state corresponding with the desired reference voltage. These include the loop control, gas distribution, and gas–wall interaction. This evolution can be described by considering the process within a single hysteresis curve.

A second group comprises effects changing the current–voltage relation. These include the deposition of an insulating layer onto the chamber walls and target erosion. The changes are not accounted for in models of the hysteresis curve. This results in a slow drift of process parameters, which is effectively described as a shift or deformation of the corresponding hysteresis curve. Applying corrections, such as subtracting the measured floating potential, can prevent this shift, significantly accelerating the stabilization of oxygen flow and gas pressure.

To achieve reproducible measurement or deposition during feedback control, all processes outlined in this study must be properly accounted for. This was demonstrated for hysteresis measurement, revealing a different deposition condition after feedback convergence when either starting from a metallic or poisoned target, known as double hysteresis. Based on the information acquired on the convergence of process conditions as presented in this study, we provide for the reader interested in correctly measuring hysteresis curves, a detailed description of this procedure (Supplementary information).

CRediT authorship contribution statement

J. Van Bever: Writing – review & editing, Writing – original draft, Methodology, Investigation, Formal analysis, Data curation. **K. Strijckmans:** Writing – review & editing, Supervision. **S. Konstantinidis:** Writing – review & editing, Resources. **D. Depla:** Writing – review & editing, Writing – original draft, Resources, Project administration, Funding acquisition, Conceptualization.

Declaration of competing interest

The authors declare that they have no known competing financial interests or personal relationships that could have appeared to influence the work reported in this paper.

Acknowledgments

The authors wish to acknowledge Ghent University for the financial support through the project TIMERS (grant number 01J05319). S. Konstantinidis is Research Director of the National Fund for Scientific Research (FRS - FNRS Belgium). We would like to thank Ing. Lode Tassignon for the co-development of the process control software and Stefaan Broekaert for the co-development of the home-build setup and the floating potential probe. The first author would also like to thank his family and loved ones for always supporting him.

Appendix A. Supplementary data

Supplementary material related to this article can be found online at https://doi.org/10.1016/j.surfcoat.2025.132095.

Data availability

Data will be made available on request.

References

[1] W.D. Sproul, D.J. Christie, D.C. Carter, Control of reactive sputtering processes, Thin Solid Films 491 (1) (2005) 1–17, http://dx.doi.org/10.1016/j.tsf.2005.05.022.

[2] G. Savorianakis, K. Mita, T. Shimizu, S. Konstantinidis, M. Voué, B. Maes, VO_2 nanostripe-based thin film with optimized color and solar characteristics for smart windows, J. Appl. Phys. 129 (18) (2021) 185306, http://dx.doi.org/10.1063/5.0049284.

[3] A. Okamoto, T. Serikawa, Reactive sputtering characteristics of silicon in an Ar-N_2 mixture, Thin Solid Films 137 (1) (1986) 143–151, http://dx.doi.org/10.1016/0040-6090(86)90202-6.

[4] C.I. van Emmerik, W.A.P.M. Hendriks, M.M. Stok, M. de Goede, L. Chang, M. Dijkstra, F. Segerink, D. Post, E.G. Keim, M.J. Dikkers, S.M. García-Blanco, Relative oxidation state of the target as guideline for depositing optical quality RF reactive magnetron sputtered Al_2O_3 layers, Opt. Mater. Express 10 (6) (2020) 1451–1462, http://dx.doi.org/10.1364/OME.393058.

[5] I. Safi, Recent aspects concerning DC reactive magnetron sputtering of thin films: a review, Surf. Coat. Technol. 127 (2) (2000) 203–218, http://dx.doi.org/10.1016/S0257-8972(00)00566-1.

[6] M. Vergöhl, B. Hunsche, N. Malkomes, T. Matthée, B. Szyszka, Stabilization of high-deposition-rate reactive magnetron sputtering of oxides by in situ spectroscopic ellipsometry and plasma diagnostics, J. Vac. Sci. Technol. A 18 (4) (2000) 1709–1712, http://dx.doi.org/10.1116/1.582412.

[7] M. Vergöhl, N. Malkomes, T. Matthée, G. Bräuer, Real time control of reactive magnetron-sputter deposited optical filters by in situ spectroscopic ellipsometry, Thin Solid Films 377–378 (2000) 43–47, http://dx.doi.org/10.1016/S0040-6090(00)01382-1.

[8] N. Malkomes, M. Vergöhl, Dynamic simulation of process control of the reactive sputter process and experimental results, J. Appl. Phys. 89 (1) (2001) 732–739, http://dx.doi.org/10.1063/1.1328407.

[9] M.A. George, E.A. Craves, R. Shehab, K. Knox, Analysis of closed loop control and sensor for a reactive sputtering drum coater, J. Vac. Sci. Technol. A 22 (4) (2004) 1804–1809, http://dx.doi.org/10.1116/1.1738661.

[10] C. Woelfel, P. Awakowicz, J. Lunze, Robust high-gain control of nonlinear reactive sputter processes, in: 2017 IEEE Conference on Control Technology and Applications, CCTA, IEEE, 2017, pp. 25–30, http://dx.doi.org/10.1109/CCTA.2017.8062435.

[11] C. Woelfel, S. Kockmann, P. Awakowicz, J. Lunze, Neural network based linearization and control of sputter processes, in: 2017 11th Asian Control Conference, ASCC, 2017, pp. 2831–2836, http://dx.doi.org/10.1109/ASCC.2017.8287626.

[12] C. Woelfel, D. Bockhorn, P. Awakowicz, J. Lunze, Model approximation and stabilization of reactive sputter processes, J. Process Control 83 (2019) 121–128, http://dx.doi.org/10.1016/j.jprocont.2018.06.009.

[13] J. Affinito, R.R. Parsons, Mechanisms of voltage controlled, reactive, planar magnetron sputtering of al in Ar/N_2 and Ar/O_2 atmospheres, J. Vac. Sci. Technol. A 2 (3) (1984) 1275–1284, http://dx.doi.org/10.1116/1.572395.

[14] K. Strijckmans, R. Schelfhout, D. Depla, Tutorial: Hysteresis during the reactive magnetron sputtering process, J. Appl. Phys. 124 (24) (2018) 241101, http://dx.doi.org/10.1063/1.5042084.

[15] J. Van Bever, K. Strijckmans, D. Depla, A computational study of the double hysteresis phenomenon during reactive sputtering, J. Phys. D: Appl. Phys. 55 (35) (2022) 355302, http://dx.doi.org/10.1088/1361-6463/ac761c.

[16] J. Van Bever, K. Strijckmans, D. Depla, Influence of chemisorption on the double hysteresis phenomenon during reactive sputtering, Appl. Surf. Sci. 613 (2023) 155901, http://dx.doi.org/10.1016/j.apsusc.2022.155901.

[17] J. Van Bever, P. Vašina, R. Drevet, K. Strijckmans, D. Depla, Floating potential probes for process control during reactive magnetron sputtering, Surf. Coat. Technol. 494 (2) (2024) 131405, http://dx.doi.org/10.1016/j.surfcoat.2024.131405.

[18] R. Schelfhout, K. Strijckmans, D. Depla, The existence of a double S-shaped process curve during reactive magnetron sputtering, Appl. Phys. Lett. 109 (11) (2016) 111605, http://dx.doi.org/10.1063/1.4962958.

[19] M.A. Lewis, D.A. Glocker, J. Jorne, Measurements of secondary electron emission in reactive sputtering of aluminum and titanium nitride, J. Vac. Sci. Technol. A 7 (3) (1989) 1019–1024, http://dx.doi.org/10.1116/1.576222.

[20] A. Belkind, A. Freilich, R. Scholl, Pulse duration effects in pulse-power reactive sputtering of Al_2O_3, Surf. Coat. Technol. 108–109 (1998) 558–563, http://dx.doi.org/10.1016/S0257-8972(98)00635-5.

[21] A. Segers, D. Depla, K. Eufinger, J. Haemers, R. De Gryse, Arc discharges in the reactive sputtering of electrical insulating compounds, in: 45th Annual Technical Conference Proceedings, Society of Vacuum Coaters, Albuquerque, 2002, pp. 30–35, URL https://www.svc.org/clientuploads/directory/resource_library/02_030.pdf.

[22] M. Meissner, T. Tolg, P. Baroch, J. Musil, Elimination of arcing in reactive sputtering of Al_2O_3 thin films prepared by DC pulse single magnetron, Plasma Process. Polym. 8 (6) (2011) 500–504, http://dx.doi.org/10.1002/ppap.201000208.

[23] N.D. Madsen, B.H. Christensen, S. Louring, A.N. Berthelsen, K.P. Almtoft, L.P. Nielsen, J. Bøttiger, Controlling the deposition rate during target erosion in reactive pulsed DC magnetron sputter deposition of alumina, Surf. Coat. Technol. 206 (23) (2012) 4850–4854, http://dx.doi.org/10.1016/j.surfcoat.2012.05.070.
[24] D. Depla, K. Strijckmans, R. De Gryse, The role of the erosion groove during reactive sputter deposition, Surf. Coat. Technol. 258 (2014) 1011–1015, http://dx.doi.org/10.1016/j.surfcoat.2014.07.038.
[25] P. Mareš, S. Kadlec, M. Dubau, A. Marek, J. Vyskočil, Long-term stability and disappearing anode effects during reactive DC and pulsed bipolar magnetron sputtering of Al_2O_3, Vacuum 173 (2020) 109161, http://dx.doi.org/10.1016/j.vacuum.2019.109161.
[26] S. Schiller, U. Heisig, K. Steinfelder, J. Strümpfel, R. Voigt, R. Fendler, G. Teschner, On the investigation of D.C. plasmatron discharges by optical emission spectrometry, Thin Solid Films 96 (3) (1982) 235–240, http://dx.doi.org/10.1016/0040-6090(82)90247-4.
[27] J.C. Sagás, L.C. Fontana, H.S. Maciel, Influence of electromagnetic confinement on the characteristics of a triode magnetron sputtering system, Vacuum 85 (6) (2011) 705–710, http://dx.doi.org/10.1016/j.vacuum.2010.11.002.
[28] K.A. Petroski, J.C. Sagás, Alternative anode geometry for magnetron sputtering, Vacuum 182 (2020) 109703, http://dx.doi.org/10.1016/j.vacuum.2020.109703.
[29] V. Bellido-González, B. Daniel, J. Counsell, M. Stevens, Flexible Reactive Gas Sputtering Process Control, Tech. Rep., Gencoa Ltd, 2008.
[30] R.M. Phelan, Pseudo-Derivative-Feedback (PDF) Control, Tech. Rep., California Univ. Livermore. Lawrence Radiation Lab, 1971, http://dx.doi.org/10.2172/4711540.
[31] R.M. Phelan, Automatic Control Systems, Cornell University Press, London, 1977, URL https://books.google.be/books?id=9s9SAAAAMAAJ.
[32] F. Golnaraghi, B.C. Kuo, Automatic Control Systems, McGraw-Hill Education, New York, 2017, URL https://www.accessengineeringlibrary.com/content/book/9781259643835.
[33] W.S. Cleveland, Robust locally weighted regression and smoothing scatterplots, J. Amer. Statist. Assoc. 74 (368) (1979) 829–836, http://dx.doi.org/10.1080/01621459.1979.10481038.
[34] S. Berg, T. Nyberg, Fundamental understanding and modeling of reactive sputtering processes, Thin Solid Films 476 (2) (2005) 215–230, http://dx.doi.org/10.1016/j.tsf.2004.10.051.
[35] K. Strijckmans, Modeling the Reactive Magnetron Sputtering Process (phdthesis), Ghent University, 2015, URL http://hdl.handle.net/1854/LU-6961940.
[36] S. Berg, E. Särhammar, T. Nyberg, Upgrading the "Berg-model" for reactive sputtering processes, Thin Solid Films 565 (2014) 186–192, http://dx.doi.org/10.1016/j.tsf.2014.02.063.
[37] W. De Bosscher, S. Van Hove, Erosion profile compensated magnetron with moving magnet assembly, application number: 99870127.0, 2008.
[38] M. Audronis, V. Bellido-Gonzalez, B. Daniel, Control of reactive high power impulse magnetron sputtering processes, Surf. Coat. Technol. 204 (14) (2010) 2159–2164, http://dx.doi.org/10.1016/j.surfcoat.2009.11.040.
[39] M. Audronis, V. Bellido-Gonzalez, Hysteresis behaviour of reactive high power impulse magnetron sputtering, Thin Solid Films 518 (8) (2010) 1962–1965, http://dx.doi.org/10.1016/j.tsf.2009.12.011.